Research Article | Vol. 27, No. 23 / 11 November 2019 / Optics Express 32958
Optics EXPRESS

Ultra-wideband terahertz metamaterial absorber based on Snowflake Koch Fractal dielectric loaded graphene

MILAD NOURBAKHSH, EHSAN ZAREIAN-JAHROMI,* AND RAHELEH BASIRI

Department of Electrical and Electronics Engineering, Shiraz University of Technology, Shiraz, Iran
**Zareian@sutech.ac.ir*

Abstract: In this paper, an ultra-wideband terahertz metamaterial absorber is introduced based on a Snowflake Koch Fractal (SKF) dielectric loaded on a sheet of graphene. Instead of multilayered-graphene conventional structures, a single-layered non-structured graphene absorber is presented based on gradient width modulation and cavity method. The structure of the absorber is composed of four layers, which are upper SKF dielectric and metal film layer form two mirrors of an asymmetric Fabry-Perot cavity to confine terahertz electromagnetic (EM) waves. Full wave simulations demonstrate that the proposed structure is highly efficient whereas a 161% fractional bandwidth of over 0.9 absorbance is achieved under normal incident wave considering both TE and TM polarizations. The proposed structure is polarization insensitive yielding the same absorbance for both TE and TM polarizations. The absorbance and bandwidth of the structure is almost independent of altering the incident angle θ up to 60° and 30° for TM and TE polarizations, respectively. Avoiding graphene processing and simple shape geometry are the interesting advantages of this structure resulting in feasible fabrication. The proposed structure provides much greater absorbance bandwidth in comparison to previous works.

1. Introduction

Terahertz spectra (THz) (100 GHz-10 THz) has been treated as a bandgap according to lack of powerful sources and detectors [1]. Recent attempts toward developing THz sources resulted in promoting researches on this frequency regime of electromagnetic spectra [2]. Gradually, THz region has attracted great attentions due to its wide range of applications such as communication, spectroscopy, sensing, and imaging [3–5]. Among all THz devices, absorbers play an important role due to necessity of wave absorption in various applications including detecting [6], imaging [7], and modulating [8].

Few materials in nature can respond to terahertz frequency. Hence, metamaterials (MMs), defined as artificial effectively homogeneous electromagnetic structures, are utilized to deal with THz [9]. To design MMs terahertz structures, the effective homogeneous condition must be satisfied. It means that the structure dimensions must be considered less than a quarter of guided wavelength. In this case, the structure can be considered as a real material [10]. The first perfect metamaterial absorber (MA) has been proposed by Landy *et al.* [11]. After that different MAs have been designed in relevant spectral range including millimeter-wave [12], IR [13], terahertz [14], and optical [15] regimes. Changing the geometry size of an absorber can result in controlling the corresponding response. However, this method suffers from practical applicability. According to this issue, it is desired to find a suitable material with demanding practical applicability and tunability features. Therefore, graphene as a single layer two dimensional honey-comb lattice of carbon atoms has been utilized as a good candidate providing these interested features.

Recently, graphene has attracted many interests according to its interesting mechanical, chemical, and electrical properties. Small thickness, high flexibility and persistence, low losses,

#373531 https://doi.org/10.1364/OE.27.032958
Journal © 2019 Received 23 Jul 2019; revised 3 Oct 2019; accepted 21 Oct 2019; published 28 Oct 2019

Optics EXPRESS

high electron mobility, and more importantly adjustable conductivity by modifying its Fermi energy according to the external DC voltage are the interesting demanded features of graphene [16].

Various broadband graphene-based absorbers with different structures have been proposed recently. In [17], L. Ye *et al.* proposed a broadband THz absorber utilizing a net-shaped graphene sheet with sinusoidal pattern. By utilizing a graphene sheet with gradient modulation and continuous plasmon resonances, the achieved bandwidth of over 0.9 absorbance is 65% considering normal incidence in case of TE and TM polarizations. A broadband tunable metamaterial absorber is proposed in [18] based on gradient diameter modulation of the graphene sheet and circular symmetry of utilized unit cell. In [19] F. Gao *et al.* presented a THz absorber with 0.82 THz bandwidth of over 90% absorption together with 1.68 THz central frequency. Y. Cai and K.-D.Xu, proposed a multilayer graphene structure by which 0.76 THz absolute bandwidth of over 90% absorbance is achieved [20]. J. Yang *et al.* presented a broadband THz absorber including a non-structured graphene layer loaded with dielectric arrays. The obtained relative bandwidth is 65% considering over 90% absorption performance [21].

In this paper, a Snowflake Koch Fractal (SKF) dielectric loaded on a sheet of graphene is utilized to obtain a broadband graphene-based absorber in THz regime. Graphene processing is avoided in design procedure and hence, the significant achievement of easy fabrication is resulted. Graphene surface plasmons (GSPs) are excited due to confined THz electromagnetic (EM) waves. These confined waves result from an asymmetric Fabry-Perot cavity. Two mirrors of the embedded Fabry-Perot cavity are realized by arrays of SKF dielectric together with a metal film. Moreover, the demanded absorption bandwidth is improved by continuous plasmon resonances provided by sharp points and gradient width parts of utilized dielectric layer. The presented structure is investigated based on full-wave simulations. Under normal incidence of both TE and TM polarizations, an ultra-wideband absorption with relative bandwidth of 161% is achieved. The proposed structure is polarization insensitive and simple to fabricate. The absorbance and the bandwidth remain stable with variation of incident angle θ between 0-60° and 0-30° for TM and TE polarizations, respectively. Therefore, the designed structure has a great potential in sensing, detecting, and optoelectronic applications.

The paper is organized as follows. Section 2 describes the geometry design and simulation methods of the structure. Section 3 discusses absorption characteristics of the structure including absorption spectra, field distributions, and electrostatic tunabilities. Finally, the paper is concluded in Section 4.

2. Design and geometry of proposed structure

The proposed ultra-wideband absorber is demonstrated in Fig. 1 where θ is the incident angle; φ is azimuth angle, and $\bar{k}$ is the wave vector. Moreover, q indicates the period of the structure in x and y directions whereas t_d, t_s, d_g, and t_g are the thickness of upper dielectric, separating dielectric, graphene sheet, and gold film, respectively. The proposed structure comprises a SKF dielectric which is mounted on top with $\varepsilon_r = 12$ provided approximately by silicon in THz range [22]. As a separating material, a low loss polyethylene cyclic olefin copolymer (Topas) with nearly constant refractive index in terahertz regime ($\varepsilon_r = 2.35$) is chosen to provide a broadband absorption [23]. This separating material is supported by a reflector gold layer defined by Drude model (relative permittivity of $\varepsilon(\omega)=\varepsilon_\infty-\omega_p^2/(\omega^2+j\omega\gamma)$ where $\varepsilon_\infty=1$, $\omega_p=1.38\times10^{16}$ rad.s^{-1} is plasma frequency, ω is angular frequency, and $\gamma = 1.23 \times 10^{13} s^{-1}$ is collision frequency) [24].

The graphene layer is modeled as an anisotropic material. Considering the graphene as a bulk material with small thickness of d_g=1 nm together with frequency ω and free space permittivity of ε_0, the complex permittivity is defined as follows [25],

$$\varepsilon_G = \varepsilon_{Gr} + j\varepsilon_{Gim} = \left(\frac{\sigma_{Gim}}{\omega d_g} + \varepsilon_0\right) + j\left(-\frac{\sigma_{Gr}}{\omega d_g}\right), \tag{1}$$

Optics EXPRESS

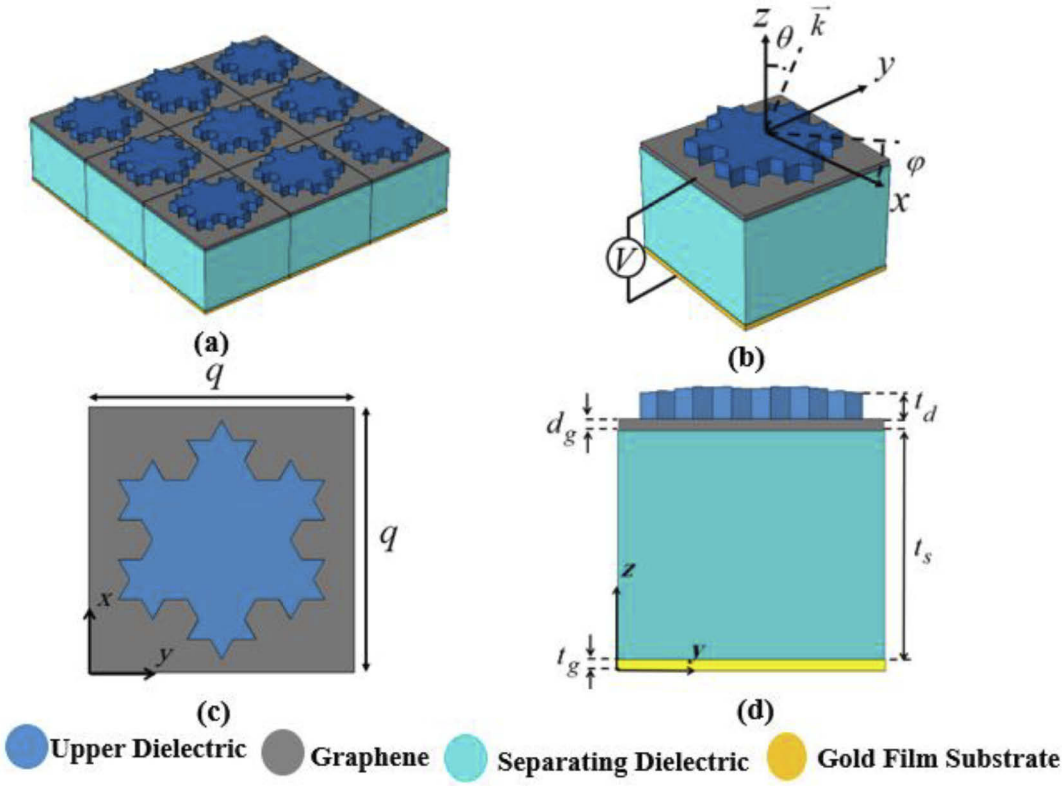

Fig. 1. (a) Proposed periodic graphene-based terahertz absorber. (b) perspective view, (c) top view, (d) side view of corresponding unit cell.

where the graphene complex conductivity $\sigma_G=\sigma_{Gr}+j\sigma_{Gim}$, can be derived by well-known Kubo formula as follows [25],

$$\sigma_G(\omega, \mu_c, \tau, T) = \sigma_{\text{intra}} + \sigma_{\text{inter}}, \tag{2}$$

$$\sigma_{\text{intra}} = \frac{-j}{\omega - j\tau^{-1}} \frac{e^2 K_B T}{\pi\hbar^2} \left(\frac{\mu_c}{K_B T} + 2\ln\left(e^{-\frac{\mu_c}{K_B T}} + 1\right)\right), \tag{3}$$

$$\sigma_{\text{inter}} = \frac{-j(\omega - j\tau^{-1})e^2}{\pi\hbar^2} \int_0^\infty \frac{f(-\varepsilon) - f(+\varepsilon)}{(\omega - j\tau^{-1})^2 - 4(\varepsilon/\hbar)^2} d\varepsilon, \tag{4}$$

where e is the electron charge, $\hbar$ is the reduced Plunk constant, K_B is the Boltzmam constant, T is the temperature, and $f(\varepsilon) = 1/\{1 + \exp[(\varepsilon\text{-}\mu_c)/(K_B T)]\}$ is the Fermi-Dirac distribution function. Moreover, μ_c is the chemical potential related to density of charge carriers and can be tuned by applying electrostatic bias field or chemical doping wheras τ is the electron relaxation time of the graphene. Since the interband contribution of graphene conductivity is negligible in THz regime, the graphene conductivity can be derived as follows,

$$\sigma_{G-intra} = \frac{-j}{\omega - j\tau^{-1}} \frac{e^2 K_B T}{\pi\hbar^2} \left(\frac{\mu_c}{K_B T} + 2\ln\left(e^{-\frac{\mu_c}{K_B T}} + 1\right)\right). \tag{5}$$

In full-wave simulations, $T = 300$ K and μ_c=0.5 eV are assumed whereas relaxation time of graphene is considered as τ=0.1 ps. The resulting absorbance is derived using the corresponding

Optics EXPRESS

S-parameters as follows [21],

$$A = 1 - T - R, \tag{6}$$

where T and R are transmission and reflection coefficients, respectively. The absorbance and S-parameters are derived using CST Microwave Studio software in which frequency domain solver is selected. Moreover, unit cell boundary conditions toward x and y directions are chosen. According to (6), minimizing the transmission and reflection coefficients leads to high achieved absorption spectrum. The SKF dielectric arrays and metal film layer form two mirrors of an asymmetric Fabry-Perot cavity which dramatically confines electromagnetic waves in the structure [26]. A thin gold film is utilized at bottom of the substrate layer to minimize the transmission coefficient. It is noted that gold layer results in zero transmission coefficient. The thickness of the gold layer is determined according to the corresponding skin depth value in THz regime (t_g=1 μm) to avoid surface currents. The thicknesses of separating and upper dielectric layers are optimized to obtain impedance matching in order to minimizing structure reflection coefficient. As a result, t_s=20 μm and t_d=3 μm are obtained. Since a single layer of graphene is transparent, in order to obtain high absorption in accordance with mutual effects of adjacent unit cells, we proposed a periodic structure with periodicity of $q = 30$ μm.

Figure 2 illustrates the design procedure of SKF dielectric utilized in the designed absorber. Graphene surface plasmons are excited, when wave vectors of free space and those of GSPs are equal. The wave vector of surface plasmon propagation along a graphene sheet is as follows [27],

$$k_{GSP}(\omega) = \frac{\pi\hbar^2}{e^2 E_f}\varepsilon_0(\varepsilon_s + \varepsilon_d)\omega(\omega + j\tau^{-1}), \tag{7}$$

where E_f is the Fermi energy of graphene, ε_s is the relative permittivity of separating dielectric, and ε_d is relative permittivity of periodic SKF dielectric. Excited GSP modes propagate through the structure. In the interface between SKF dielectric and air gap, they proportionally reflect back whereas some of them transmit into the air to re-excite GSPs in the next cell. Since the distance between two adjacent SKF dielectrics is smaller than corresponding wavelength, more effective far field interactions become available [19,27].

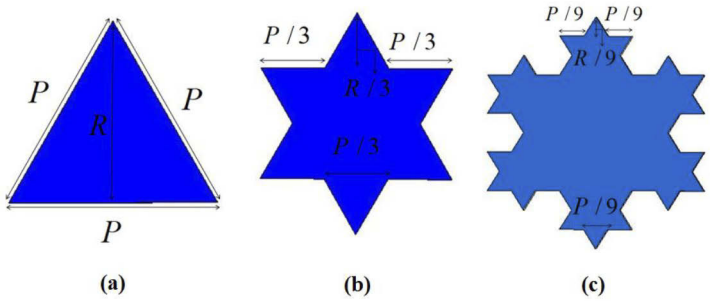

Fig. 2. Different iteration of snowflake Koch curve (a) 0^{th} order iteration (b) 1^{st} order iteration (c) 2^{nd} order iteration with parameters: $P = 23$μm and $R = P\sqrt{3}/2$ [28].

3. Results and discussion

The upper SKF dielectric layer is utilized to obtain wideband absorption through continuous excitation of surface plasmons on graphene layer. First, we investigate the 0^{th} order of SKF as an upper dielectric (Fig. 2(a)).

As can be seen in Fig. 3, the corresponding absorption spectra include many unwanted variations dropping at 6 THz and 5.54 THz for TE and TM polarizations, respectively. Hence,

Optics EXPRESS

the 1st order of the SKF is investigated (Fig. 2(b)). Figure 4 indicates the absorption spectra corresponding to the second structure. For TE polarization, broadband absorption of 159% is achieved whereas the absorption magnitude shows a reduction under 0.9 at 7.42 THz considering TM polarization.

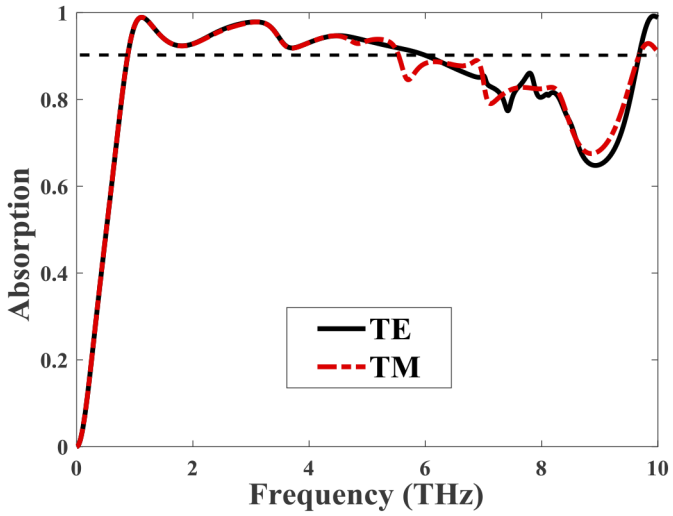

Fig. 3. Absorption spectra corresponding to the 0th order structure in Fig. 2(a) for TE and TM polarization under normal incidence considering μ_c=0.5 eV.

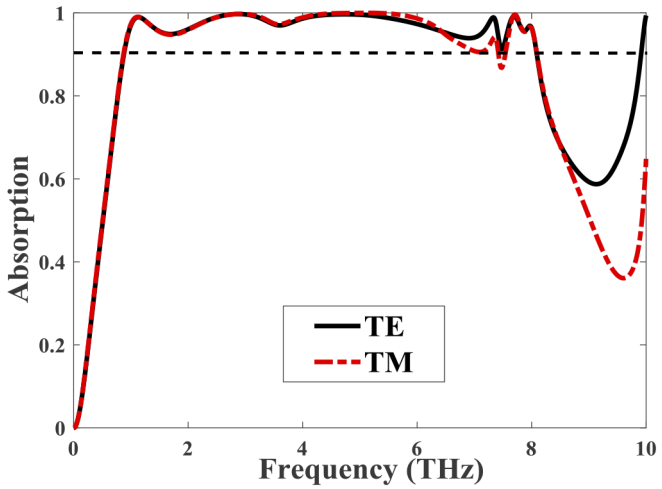

Fig. 4. Absorption spectra corresponding to the 1st order structure in Fig. 2(b) for TE and TM polarization under normal incidence considering $\mu_c = 0.5$ eV.

Finally, 2nd order SKF is chosen to improve the absorption behavior. The broadband achievement follows two working mechanisms. First, discrete graphene plasmon resonances are produced by the non-structured graphene loaded with SKF dielectric. Second, there is a set of continuous plasmon resonances due to gradually variation of the SKF dielectric width [21]. The proposed absorber is designed based on gradient width modulation of upper dielectric. The higher iterations of SKF include more gradient width sections. The 2nd order SKF dielectric can

Optics EXPRESS

be divided into infinite infinitesimal trapezoids along x direction in which, each pair of lateral infinitesimal faces along y direction act as two mirrors of a Fabry-Perot cavity (Fig. 5). Therefore, continuous plasmon resonances are obtained resulting in improved absorption bandwidth.

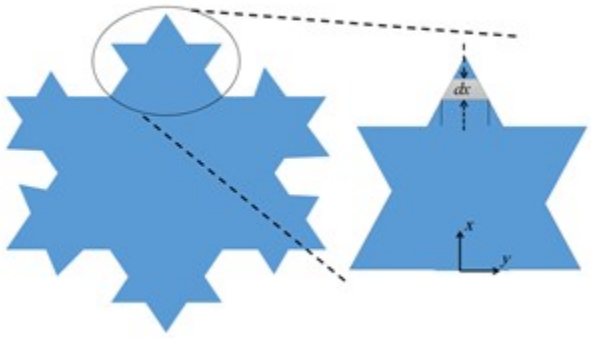

Fig. 5. 2nd order SKF in Fig. 2(c) divided into infinite infinitesimal trapezoids along x direction.

The absorption spectra and field distributions are investigated considering normal incidence. Figure 6 indicates the absorption spectra for both TE and TM polarizations. All investigated structures are analyzed under assumption of μ_c=0.5 eV for graphene layer. A wide over 0.9 absorption performance in the range of 0.88-8.12 THz is achieved for both TE and TM polarizations. It is noted that the central frequency and relative bandwidth are 4.5 THz and 161%, respectively. The absorption curves are almost similar for both polarizations whereas minor discrepancies are observed due to different resonance length values in x and y directions. Figure 7 demonstrates the electric field distributions at the interface of upper SKF and graphene sheet for both polarizations at 0.3 THz, 4.5 THz, and 9 THz.

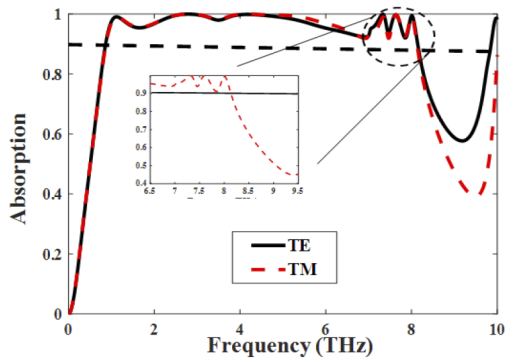

Fig. 6. Absorption spectra corresponding to the 2nd order structure in Fig. 2(c) for TE and TM polarization under normal incidence considering μ_c=0.5 eV.

According to Fig. 7, electric fields are mostly confined at the edge of the SKF dielectric layer due to the excitation of localized surface plasmons of graphene. In TM and TE polarizations, the plasmon resonances are in y and x directions which are in accordance with the polarization of corresponding incident wave. It is noted that the more electric fields confinement, the more absorption achievement. Thus, unity absorption obtained at 4.5 THz for both polarizations is in accordance with corresponding maximum electric fields confinement (Fig. 7(b) and 7(e)).

Optics EXPRESS

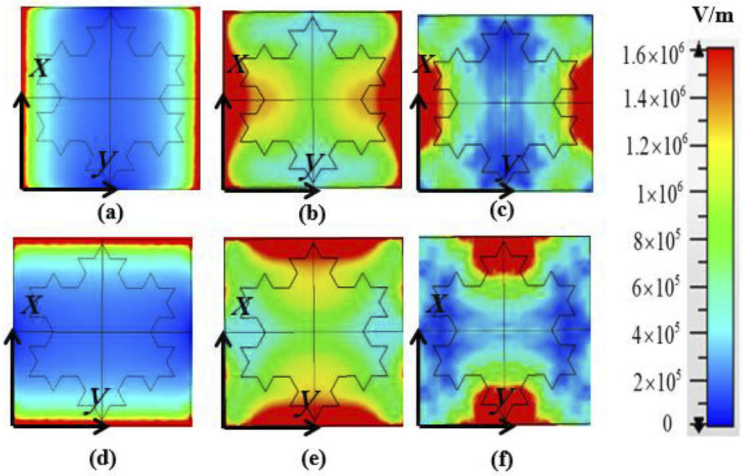

Fig. 7. Electric field distribution of Fig. 1 considering μ_c=0.5 eV at the interface of snowflake Koch dielectric and graphene for TM polarization at frequency of (a) 0.3 THz (b) 4.5 THz (c) 9 THz and for TE polarization at frequency of (d) 0.3 THz (e) 4.5 THz (f) 9 THz.

Moreover, decreasing the fields confinement results in reduced absorption intensity at 9 THz (Fig. 7(c) and 7(f)). At 0.3 THz (Fig. 7(a) and 7(d)) only the edge resonances between adjacent unit cells are observed and hence, the absorption intensity is declined.

The impact of altering the structure periodicity is investigated in Fig. 8. As q is varied between 28-30μm, the impedance matching condition is more satisfied and hence, absorbance bandwidth and corresponding intensity increase. If the periodicity increasing continues between 30-32 μm, the impedance matching is deteriorated and as a consequence, the absorption spectra encounter a falling trend.

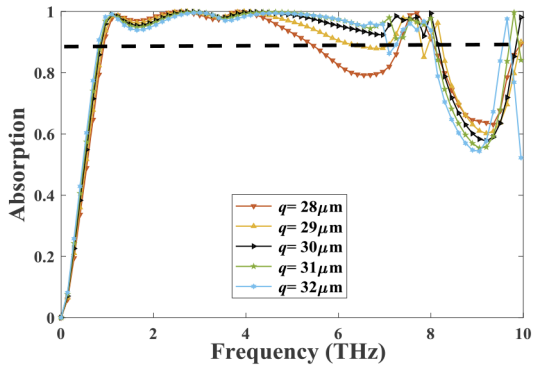

Fig. 8. Absorbance of the proposed structure in Fig. 1 considering t_s=20 μm, t_d=3 μm, and different q values.

It is worth to point out that a high electric field is confined between two adjacent unit cells in x and y directions. The electric field distribution is illustrated in Fig. 9(a) and 9(b) in yz plane for TM polarization and in xz plane for TE polarization. Optimizing structure dimensions leads to coupling effects between adjacent unit cells. Therefore, y-polarized TM and x-polarized TE incident waves excite electric dipole resonances in y and x directions.

Optics EXPRESS

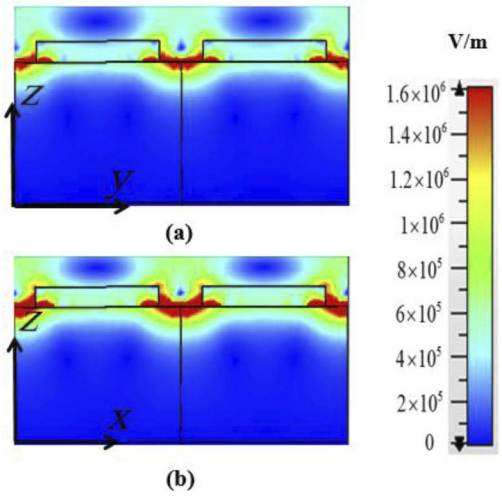

Fig. 9. Electric field distribution at the center of structure in Fig. 1 considering two adjacent unit cells in (a) *yz* plane and (b) *xz* plane.

The absorption spectra of the proposed structure for different thicknesses of separating dielectric and upper SKF dielectric are investigated in Fig. 10. It is obvious that the best absorption performance is achieved considering t_s=20 μm and t_d=3 μm.

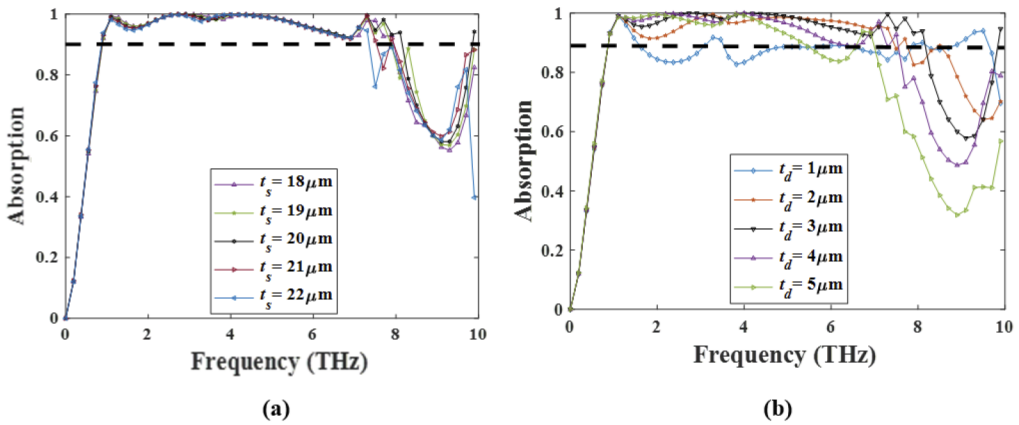

Fig. 10. Absorbance of the proposed structure for different thicknesses of (a) separating dielectric when q = 30 μm, and t_s=*3 μm* (b) upper Snowflake Koch Fractal dielectric when q = 30 μm, and t_s=20 μm.

As can be seen from Fig. 10(a), the absorbance bandwidth increases as t_s varies between 18-20 μm. However, the absorption bandwidth tends to drop slightly as t_s increases between 20-22 μm. Likewise, the same holds true for the variation of t_d. Figure 10(b) illustrates that the better absorption bandwidth is achieved whereas t_d increases between 1-3 μm. However, the absorption spectrum is deteriorated when the thickness of upper SKF dielectric varies between 3-5 μm. This is due to the fact that as t_d increases, the impedance matching between absorber structure and free space is destroyed.

The absorbance and bandwidth of the proposed structure can be modified slightly by changing the incident angle θ. This is presented in Fig. 11 where the absorption intensity is demonstrated

Optics EXPRESS

with respect to θ and frequency for both TE and TM polarizations. The graph reveals that the absorbance peak and bandwidth decrease slightly over a wide range of incident angle θ for both polarizations. It is almost stable when θ varies between 0-60° for TM polarization. TE excitement remains unchanged according to variation of θ between 0-30°. In case of TE polarization, the absorption spectra deteriorate much faster as θ increases. This is due to the fact that, the tangential component of the electric field decreases as θ increases resulting in decreasing of electric dipole resonance of the graphene.

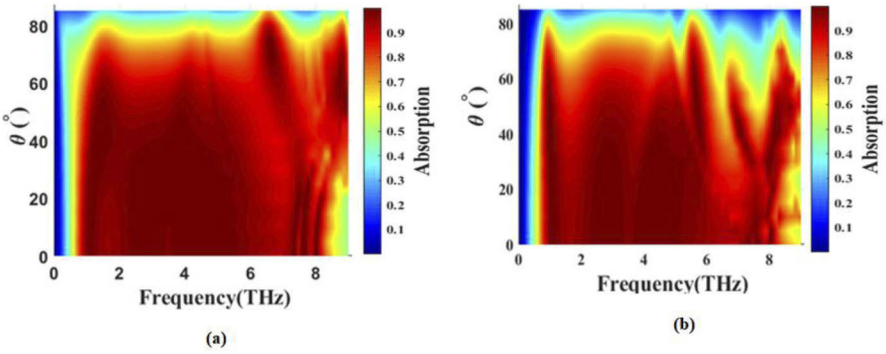

Fig. 11. Absorbance of the proposed structure in Fig. 1 as a function of frequency and incident angle for (a) TM polarization and (b) TE polarization.

It is worth to note that the absorption spectra are independent of the variation of φ due to applied symmetry in designed structure considering both TE and TM polarizations. The stability of the structure response versus changing φ and polarization results in a demanded candidate for sensing, detecting, and optoelectronic applications.

Figure 12(a) indicates the effects of μ_c on absorption spectra as graphene chemical potential is varied by electrostatic doping from 0 to 0.9 eV utilizing ion-gel top gating method [29]. The mentioned method guarantees that all these chemical potential values can be applied without a break down of the gate dielectric. The absorption of the structure shows a slight blue shift as μ_c is increased. The mentioned blue shift can be described according to Kubo formula [30] in which the plasmon resonance frequency of the graphene increases as μ_c is increased. Also, the absorption of the structure decreases dramatically as μ_c varies between 0-0.2 eV. This is resulted from decreasing metallic character of graphene in lower range of μ_c.

There is an interesting phenomenon in which three peaks of over 0.8 absorbance are observed in case of $\mu_c = 0$ where there is no GSPs. Figure 12(b) demonstrates the absorption spectra of the proposed structure for $\mu_c = 0$. Considering 0.88-8.12 THz, these three absorption peaks are observed at 2.9THz, 7.19 THz, and 7.66 THz, respectively. The corresponding magnetic field distribution (Fig. 12(c)) indicates that these abnormal absorbance peaks are due to SKF dielectric resonances along x-axis.

In Table 1, the proposed structure is compared to conventional broadband graphene-based absorbers. It is obvious that the presented structure has much greater absorbance bandwidth in comparison to other works. Moreover, the significant achievement of easy fabrication is resulted due to avoiding graphene processing and considering simple shape geometry.

Optics EXPRESS

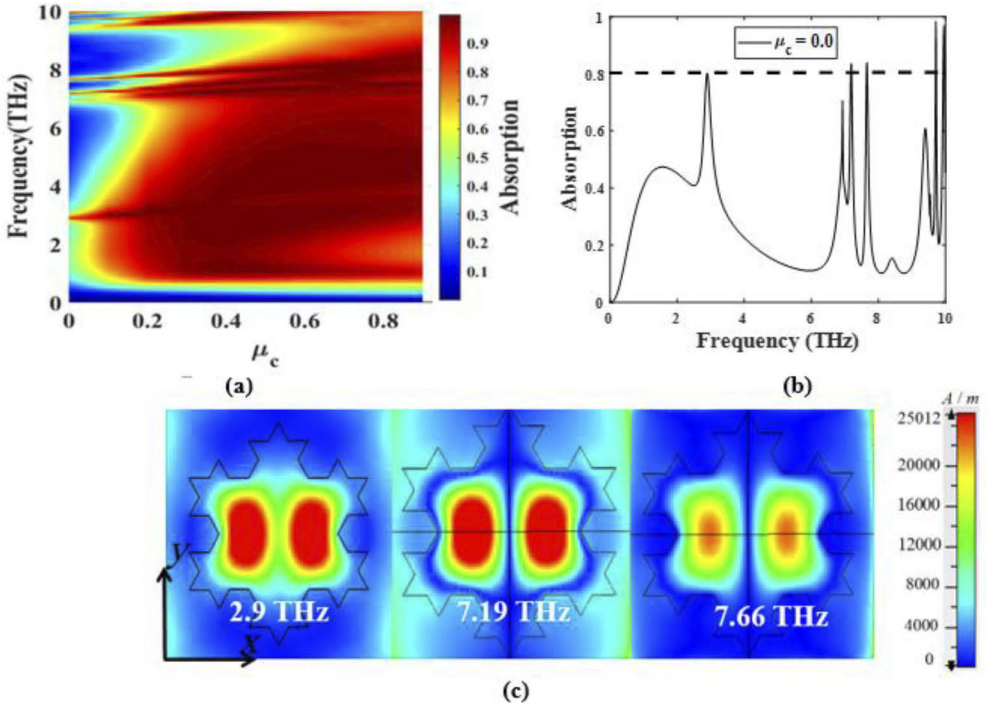

Fig. 12. Absorption spectra of the proposed absorber in Fig. 1: (a) as a function of frequency and μ_c (b) considering μ_c=0 (c) magnetic field distribution of the proposed structure for μ_c=0.

Table 1. Physical and practical characteristics

References	90% absolute bandwidth (THz)	Relative bandwidth	Unit cell dimension (μm^3)	Type	Fabrication Difficulty
[17]	1.1	65%	$60 \times 32 \times 26$	Single layer	Not Easy
[18]	1.57	86%	$75 \times 75 \times 28.2$	Single layer	Not Easy
[19]	0.82	48.8%	$40 \times 40 \times 37$	Single layer	Easy
[20]	0.76	11.4%	$0.25 \times 0.25 \times 9.5$	Multilayer	Not Easy
[21]	1.5	65%	$24 \times 80 \times 28$	Single layer	Easy
Proposed structure	7.24	161%	$30 \times 30 \times 24$	Single layer	Easy

4. Conclusion

In this manuscript, an ultra-wideband non-structured graphene-based absorber is proposed based on width modulation of a dielectric layer together with cavity method to excite continuous surface plasmons of graphene sheet. The obtained structure yields a wideband absorbance of over 0.9 between 0.88-8.12 THz. The central frequency of absorption spectra is 4.5 THz and the relative bandwidth of 161% is obtained. Under normal incidence, the absorption curve is nearly close for both TE and TM polarization resulting to an almost polarization insensitive structure. The structure is also insensitive to the angle φ due to the geometric symmetry. Moreover, the absorption spectra change gradually as θ varies between 0- 60° for TM polarization and 0-30° for TE polarization. The polarization insensitivity and stability of the absorption spectra show a great potential in sensing, detecting, and optoelectronic applications. Compared to the

Optics EXPRESS

conventional works, the proposed structure provides more wideband performance and is feasible from fabrication perspective.

References

1. K. R. Jha and G. Singh, *Terahertz planar antennas for next generation communication*. (Springer, 2014).
2. B. Ferguson and X.-C. Zhang, "Materials for terahertz science and technology," Nat. Mater. **1**(1), 26–33 (2002).
3. P. U. Jepsen, D. G. Cooke, and M. Koch, "Terahertz spectroscopy and imaging–Modern techniques and applications," Laser Photonics Rev. **5**(1), 124–166 (2011).
4. J. M. Jornet and I. F. Akyildiz, "Graphene-based plasmonic nano-antenna for terahertz band communication in nanonetworks," IEEE J. Select. Areas Commun. **31**(12), 685–694 (2013).
5. R. Singh, W. Cao, I. Al-Naib, L. Cong, W. Withayachumnankul, and W. Zhang, "Ultrasensitive terahertz sensing with high-Q Fano resonances in metasurfaces," Appl. Phys. Lett. **105**(17), 171101 (2014).
6. J. Wang, J. Gou, and W. Li, "Preparation of room temperature terahertz detector with lithium tantalate crystal and thin film," AIP Adv. **4**(2), 027106 (2014).
7. R. Yahiaoui, S. Tan, L. Cong, R. Singh, F. Yan, and W. Zhang, "Multispectral terahertz sensing with highly flexible ultrathin metamaterial absorber," J. Appl. Phys. **118**(8), 083103 (2015).
8. S. Savo, D. Shrekenhamer, and W. J. Padilla, "Liquid crystal metamaterial absorber spatial light modulator for THz applications," Adv. Opt. Mater. **2**(3), 275–279 (2014).
9. C. Caloz and T. Itoh, *Electromagnetic metamaterials: transmission line theory and microwave applications*. (John Wiley & Sons, 2005).
10. H. M. Nemat-Abad, E. Zareian-Jahromi, and R. Basiri, "Design and equivalent circuit model extraction of a third-order band-pass frequency selective surface filter for terahertz applications," Int. J. Eng. Sci. Technol. **22**(3), 862–868 (2019).
11. N. I. Landy, S. Sajuyigbe, J. J. Mock, D. R. Smith, and W. J. Padilla, "Perfect metamaterial absorber," Phys. Rev. Lett. **100**(20), 207402 (2008).
12. B. Wu, H. M. Tuncer, M. Naeem, B. Yang, M. T. Cole, M. I. Milne, and Y. Hao, "Experimental demonstration of a transparent graphene millimetre wave absorber with 28% fractional bandwidth at 140 GHz," Sci. Rep. **4**(1), 4130 (2015).
13. W. Guo, Y. Liu, and T. Han, "Ultra-broadband infrared metasurface absorber," Opt. Express **24**(18), 20586–20592 (2016).
14. X. Liu, K. Fan, I. V. Shadrivov, and W. J. Padilla, "Experimental realization of a terahertz all-dielectric metasurface absorber," Opt. Express **25**(1), 191–201 (2017).
15. C.-H. Lin, R.-L. Chern, and H.-Y. Lin, "Polarization-independent broad-band nearly perfect absorbers in the visible regime," Opt. Express **19**(2), 415–424 (2011).
16. Q. Bao, H. Hoh, and Y. Zhang, *Graphene Photonics, Optoelectronics, and Plasmonics*. (CRC Press, 2017).
17. L. Ye, Y. Chen, G. Cai, N. Liu, J. Zhu, Z. Song, and Q. H. Liu, "Broadband absorber with periodically sinusoidally-patterned graphene layer in terahertz range," Opt. Express **25**(10), 11223–11232 (2017).
18. X. Huang, W. He, F. Yang, J. Ran, B. Gao, and W.-L. Zhang, "Polarization-independent and angle-insensitive broadband absorber with a target-patterned graphene layer in the terahertz regime," Opt. Express **26**(20), 25558–25566 (2018).
19. F. Gao, Z. Zhu, W. Xu, J. Zhang, C. Guo, K. Liu, X. Yuan, and S. Qin, "Broadband wave absorption in single-layered and nonstructured graphene based on far-field interaction effect," Opt. Express **25**(9), 9579–9586 (2017).
20. Y. Cai and K.-D. Xu, "Tunable broadband terahertz absorber based on multilayer graphene-sandwiched plasmonic structure," Opt. Express **26**(24), 31693–31705 (2018).
21. J. Yang, Z. Zhu, J. Zhang, C. Guo, W. Xu, K. Liu, X. Yuan, and S. Qin, "Broadband terahertz absorber based on multi-band continuous plasmon resonances in geometrically gradient dielectric-loaded graphene plasmon structure," Sci. Rep. **8**(1), 3239 (2018).
22. L. Ju, B. Geng, J. Horng, M. Martin, Z. Hao, H. A. Bechtel, X. Liang, A. Zettl, Y. R. Shen, and F. Wang, "Graphene plasmonics for tunable terahertz metamaterials," Nat. Nanotechnol. **6**(10), 630–634 (2011).
23. P. D. Cunningham, N. N. Valdes, F. A. Vallejo, L. M. Hayden, B. Polishak, X. H. Zhuo, J. Luo, A. K. Jen, J. C. William, and R. J. Twieg, "Broadband terahertz characterization of the refractive index and absorption of some important polymeric and organic electro-optic materials," J. Appl. Phys. **109**(4), 043505 (2011).
24. Z. H. Zhu, C. C. Guo, K. Liu, W. M. Ye, X. D. Yuan, B. Yang, and T. Ma, "Metallic nanofilm half-wave plate based on magnetic plasmon resonance," Opt. Lett. **37**(4), 698–700 (2012).
25. S. E. Hosseininejad, N. Komjani, and M. T. Noghani, "A comparison of graphene and noble metals as conductors for plasmonic one-dimensional waveguides," IEEE Trans. Nanotechnol. **14**(5), 829–836 (2015).
26. R. Alaee, M. Farhat, C. Rockstuhl, and F. Lederer, "A perfect absorber made of a graphene micro-ribbon metamaterial," Opt. Express **20**(27), 28017–28024 (2012).
27. W. Xu, Z. H. Zhu, K. Liu, J. F. Zhang, X. D. Yuan, Q. S. Lu, and S. Q. Qin, "Dielectric loaded graphene plasmon waveguide," Opt. Express **23**(4), 5147–5153 (2015).

Optics EXPRESS

28. P. R. Prajapati, G. G. K. Murthy, A. Patnaik, and M. V. Kartikeyan, "Design and testing of a compact circularly polarised microstrip antenna with fractal defected ground structure for L-band applications," IET Microw. Antennas Propag. **9**(11), 1179–1185 (2015).
29. C.-F. Chen, C.-H. Park, B. W. Boudouris, J. Horng, B. Geng, C. Girit, A. Zettl, M. F. Crommie, R. A. Segalman, S. G Louie, and F. Wang, "Controlling inelastic light scattering quantum pathways in graphene," Nature **471**(7340), 617–620 (2011).
30. G. W. Hanson, "Dyadic Green's functions for an anisotropic, non-local model of biased graphene," IEEE Trans. Antennas Propag. **56**(3), 747–757 (2008).